TYPE Original Research
PUBLISHED 11 August 2025
DOI 10.3389/frvir.2025.1592287

ARchitect: advancing architectural visualization and interaction through handheld augmented reality

Sabahat Israr[1,2], Mudassar Ali Khan[3], Muhammad Shahid Anwar[4]*, Kamran Ahmad Awan[3], Saoucene Mahfoudh[5], Turki Althaqafi[6] and Wadee Alhalabi[7,8]

[1]Department of Computer Science, Government Postgraduate College for Women, Haripur, Pakistan, [2]Higher Education Department, Khyber Pakhtunkhwa, Pakistan, [3]Department of Information Technology, The University of Haripur, Haripur, Pakistan, [4]IRC for Finance and Digital Economy, King Fahd University of Petroleum and Minerals, Dhahran, Saudi Arabia, [5]School of Engineering, Computing, and Design, Dar Al-Hekma University, Jeddah, Saudi Arabia, [6]Computer Science Department, School of Engineering, Computing and Design, Dar Al-Hekma University, Jeddah, Saudi Arabia, [7]Immersive Virtual Reality Research Group, Department of Computer Science, King Abdulaziz University, Jeddah, Saudi Arabia, [8]Department of Computer Science, Dar Al-Hekma University, Jeddah, Saudi Arabia

Check for updates

OPEN ACCESS

EDITED BY
Andrea Sanna,
Polytechnic University of Turin, Italy

REVIEWED BY
Luca Ulrich,
Polytechnic University of Turin, Italy
Arnis Cirulis,
Vidzeme University of Applied Sciences, Latvia

*CORRESPONDENCE
Muhammad Shahid Anwar,
✉ muhammad.anwar.1@kfupm.edu.sa

RECEIVED 12 March 2025
ACCEPTED 03 June 2025
PUBLISHED 11 August 2025

CITATION
Israr S, Khan MA, Anwar MS, Awan KA, Mahfoudh S, Althaqafi T and Alhalabi W (2025) ARchitect: advancing architectural visualization and interaction through handheld augmented reality.
Front. Virtual Real. 6:1592287.
doi: 10.3389/frvir.2025.1592287

The architecture, engineering, and construction industry requires enhanced tools for efficient collaboration and user-centric designs. Traditional visualization methods relying on 2D/3D CAD models often fall short of modern demands for interactivity and context-aware representation. To address this limitation, this study introduces ARchitect, a mobile-based markerless augmented reality (AR) framework aimed at revolutionizing architectural artifact visualization and interaction. The proposed approach enables users to dynamically overlay and manipulate 3D architectural elements, such as roofs, windows, and doors, within their physical environment using AR raycasting and device sensors. Algorithms supporting translation, rotation, and scaling allow precise adjustments to model placement while integrating metadata to enhance design comprehension. Real-time lighting adaptation ensures seamless environmental blending, and the framework's usability is quantitatively evaluated using the Handheld Augmented Reality Usability Scale (HARUS). ARchitect achieved a usability score of 89.2, demonstrating significant improvements in user engagement, accuracy, and decision-making compared to conventional methods.

KEYWORDS

augmented reality, 3D interaction, markerless tracking, architecture, handheld AR, 3D visualization, virtual world

1 Introduction

In the Architecture, Engineering, and Construction (AEC) industry, the design process involves continuously addressing client requirements through collaborative efforts (Singh et al., 2011). The stakeholder group for the AEC sector extends beyond engineers and designers to include end-users and clients, making their feedback on design alternatives essential at every stage of a project. This iterative exchange significantly improves the quality of the design and ensures alignment with user expectations (Mohammadpour et al., 2015; East et al., 2004). Architects often work with diverse datasets that encompass natural and cultural contexts, which play a critical role in the success of an architectural design. Sitespecific spatial data, reflecting the surrounding environment, has a direct impact on the design process due to the interdependence between architectural structures and their contexts. Consequently, architects invest substantial time in analyzing the characteristics of the contextual and local site before initiating the design process (Skov et al., 2013).

The visualization of architectural models and spatial data in the AEC industry has traditionally relied on various methods and technologies. Historically, these visualizations have been presented as 2D or 3D drawings, either on paper (Spallone and Natta, 2022) or through software tools such as SketchUp (Peng et al., 2023), Autodesk (Baik, 2024), Lumion (Ratcliffe and Simons, 2017), and Revit (Seipel et al., 2020). However, these conventional approaches face significant limitations in addressing the evolving demands of the digital era (Sedlmair et al., 2014). Specifically, challenges such as the gap between data acquisition and cognition hinder the ability to sample comprehensively and visually navigate multidimensional datasets (Abdelaal et al., 2022; Knippers et al., 2021). Moreover, traditional visualization methods are time-intensive, less efficient, and lack collaborative features essential for effective stakeholder engagement. While other engineering and non-engineering domains have successfully adopted modern technologies, the AEC industry has been notably slow in embracing such advancements, as highlighted in prior research (Hadavi and Alizadehsalehi, 2024). The reason for this slowness is the AEC industry's slow adoption of modern technologies is largely due to costly investments, limited cost-effectiveness of worker training, slim profit margins, lack of decision support tools, technological incompatibility with existing workflows, and a traditionally change-resistant industry culture (Yap et al., 2022).

Immersive technologies, which expand the reality-virtuality continuum, have seen rapid adoption across various domains (Milgram et al., 1995; Anwar et al., 2024, Anwar et al., 2023). These technologies replicate realistic sensory experiences, including visual, haptic, auditory, and motion-based interactions (Um et al., 2023; Milgram and Colquhoun, 1999). At the two ends of this continuum lie reality (the physical world) and virtuality (virtual reality (VR). Positioned closer to reality is augmented reality (AR), which enables the integration of virtual content into real-world environments in real time, while augmented virtuality (AV) sits closer to virtuality. Among these, AR stands out for its ability to improve understanding by providing contextualized interactions with virtual content (Azuma, 1997). In the AEC industry, AR facilitates a collaborative environment in which engineers, designers, architects, and stakeholders can engage in planning, design, and construction with improved coordination (Wang et al., 2022). AR implementations include wearable AR glasses (Fiorillo et al., 2024), spatial AR for projecting visuals onto physical surfaces (Gheorghiu et al., 2024), and mobile AR utilizing handheld devices like smartphones and tablets (Murthy et al., 2023). Recent advancements in smartphone technology have enhanced the efficiency, usability, and accessibility of mobile AR, particularly in terms of three-dimensional rendering, processing, and tracking capabilities (Ridel et al., 2014; Butchart, 2011).

This study introduces *ARchitect*, a markerless mobile augmented reality framework designed for the AEC industry to enable visualization and interaction with 3D architectural building elements such as windows, doors, and roofs. The framework utilizes advanced AR raycasting and device sensors for precise placement and manipulation of virtual elements within real-world environments. Users can dynamically translate, rotate, and scale models to view them from multiple perspectives in their actual construction contexts. Furthermore, the system incorporates real-time lighting adjustments and metadata integration to provide detailed information about model dimensions, structural features, and contextual suitability. The proposed framework operates across various mobile platforms without requiring external hardware, ensuring broad accessibility and natural user interaction in immersive environments. The technical contributions of the proposed approach can be summarized as:

- Novel markerless AR framework enabling seamless interaction and precise placement of architectural elements in real-world environments without dependency on external markers or hardware.
- Advanced user interaction capabilities for architectural models, including real-time translation, rotation, and scaling, facilitating context-aware visualization directly at construction sites.
- Integration of metadata with real-time lighting and environmental adaptation to enhance the comprehension of architectural designs, supporting informed decision-making during the design and construction processes.

The remainder of the paper is structured as follows: In Section 1, background information and a review of the literature are presented. Our suggested framework is explained in depth in Section 3. Section 4 details the experiments we conducted and the results we obtained. Section 6 discusses the result, and our work is concluded in section 7.

2 Background and related work

The Architecture, Engineering, and Construction (AEC) industry often faces challenges in meeting budgetary, scheduling, and quality standards while managing diverse stakeholder expectations (Chao et al., 2000; Krizek and Hadavi, 2007). To address these challenges, the industry must adopt advanced technologies for visualization, data management, and collaboration (Darko et al., 2020; Han and Leite, 2022; Bassier et al., 2024). Traditional visualization methods, such as 2D or 3D models, are often shared through in-person meetings or digital platforms like Zoom or Microsoft Teams. However, these methods are inefficient, time-consuming, and do not provide the spatial and contextual essence of designs (Hadavi and Alizadehsalehi, 2024). Researchers have started to integrate extended reality technologies into AEC tasks to improve efficiency and improve outcomes (Chi et al., 2013; Panya et al., 2023; Valizadeh et al., 2024). Augmented reality (AR), a prominent extended reality technology, has gained attention for its ability to overlay digital models onto the physical world using mobile devices, eliminating the need for additional hardware (Salavitabar et al., 2023; Ayala-Nino et al., 2023; Mitterberger et al., 2020).

Several AR-based prototypes and frameworks have been developed to enhance visualization, interactivity, and immersion

TABLE 1 Description of visualization and manipulation techniques with limitations.

Ref	Contributions	Limitations
Yu et al. (2024)	Combined tangible interface, visualization, and AR for better user interaction and accuracy	Restricted to physical cards for interaction, limiting broader usability
Cakici Alp et al. (2023)	Enhanced educational methodologies and refined AR interface design	Results were not generalizable due to a small evaluation sample size
Marino et al. (2021)	Supported error detection in production by visualizing 3D models with annotations	Constrained to marker-based use; lighting conditions caused marker detection issues
Lotsaris et al. (2021)	Visualized safety data in human-robot collaborative environments	Relied on bulky HoloLens headsets, reducing comfort and negatively impacting user performance; lacked statistical validation
Ratajczak et al. (2019)	Enabled context-specific monitoring by integrating AR, BIM, and LBMS.	Prototype lacked full integration and alignment accuracy; no real-world testing was conducted
Olsen et al. (2019)	Improved coordination for embeds and penetrations in construction using AR.	Precision issues; reliance on costly HoloLens; results lacked statistical validation
Vassigh et al. (2018)	Created a collaborative learning environment for AEC students with AR/VR.	Location dependency limited usability indoors due to GPS signal unavailability
Gheisari et al. (2016)	Augmented BIM data onto panoramic construction jobsite views	Panoramic media updates were not real-time, offering a semi-AR experience
Pan and Isnaeni (2024)	Enhanced building inspection and monitoring, reduced reliance on traditional drawings	Faced challenges with precise alignment of virtual and real elements so had discrepancies between as-planned and as-built conditions
Agrawal et al. (2024)	Deployed and evaluated Digital Twin prototype in an AEC context, uncovering key technical and organizational barriers that hinder adoption in the AEC industry	Insights were drawn from a single case context
Piras et al. (2025)	Developed an interoperable Digital Twin-based IoT framework that integrates real-time sensing, predictive analytics, and automated control to optimize indoor environmental quality and energy efficiency	Did not evaluate system performance across diverse building types and lack validation in real-world deployment scenarios
*	Enabled markerless tracking using mobile AR to overlay architectural elements and enrich models with metadata	Focused solely on end-user perspective; lacks evaluation for engineers and architects

in the AEC domain. RelicCard, for example, utilized tangible interfaces for augmented reality to explore cultural relics, although it was limited to physical cards for interaction (Yu et al., 2024). Another study introduced a mixed reality platform, Fologram, for architectural students to design and display models in AR, though the small sample size limited the generalizability of the results (Cakici Alp et al., 2023). Similarly, researchers proposed frameworks for error detection in production and assembly using AR in industrial contexts, but issues like marker dependency and lighting conditions impacted usability (Marino et al., 2021; Lotsaris et al., 2021). Integration of AR with Building Information Modeling (BIM) has shown promise, but alignment errors and incomplete functionalities have restricted its full potential (Ratajczak et al., 2019; Olsen et al., 2019).

Despite these advancements, existing AR systems in AEC have notable limitations. Many rely on head-mounted displays (HMDs) that are bulky, costly, and limit accessibility to a single user (Vassigh et al., 2018; Gheisari et al., 2016). Others depend on markers or location constraints, reducing their flexibility and usability (Dong and Kamat, 2013; Chalhoub and Ayer, 2018). Moreover, several methodologies lack comprehensive evaluation or statistical testing to validate their findings (Gheisari et al., 2016; Olsen et al., 2019). A summary of related contributions and limitations is presented in Table 1, highlighting the need for a markerless mobile AR framework with greater applicability and robust validation.

3 Proposed framework

This study proposed a framework aiming to develop an intuitive and easy-to-use markerless mobile augmented reality framework supported by different mobile devices and which can provide an immersive and interactive experience to the stakeholders of the AEC industry. All the design models of architectural building elements are designed using Sketchp[1] software. For the development of the framework, Unity3D[2] and Microsoft Visual Studio[3] are used. Development is performed on a Microsoft Windows 10 laptop with an Intel(R) Core(TM) i7-7600U processor, 16 GB RAM. User testing was conducted on Infinix X697 (Android Version 11). Figure 1 illustrates the architecture of our proposed framework.

Using SketchUp, three types of architectural building elements, including roofs, doors, and windows, French were designed. Different dimensions, geometries, meshes, and use cases are considered when designing composite, louvered, flush, and french doors for various geographical regions. Similarly, different roof designs were created for butterfly, dormer, flat, gable, and

[1] https://help.sketchup.com/en/downloading-sketchup

[2] https://unity.com/download

[3] https://visualstudio.microsoft.com/downloads/

pyramid roofs. Various window types with unique features are constructed, including single-, double-hung, skylight, sliding, and transome windows. An example interface while designing the model is shown in Figure 2.

3.1 Markerless tracking to overlay 3D architectural building elements

The markerless tracking mechanism in our proposed framework leverages advanced augmented reality techniques to overlay 3D architectural building elements onto real-world surfaces. The detailed process for markerless tracking and overlaying 3D architectural building elements is outlined in Algorithm 1.2

```
Input: $T$: Set of touch inputs (Equation 1)
       $H$: Detected hit results (Equation 1)
       $R_{cm}$: AR Raycast Manager (Equation 1)
       $P_s$: Prefabricated 3D Model (Equation 1)
       $\mathbf{p}_c$: Camera position (Equation 5)
       $\mathbf{d}$: Ray direction (Equation 5)
Output: Overlayed 3D architectural model at desired position
Initialize empty hit list $H$;
if number of touch inputs $T > 0$ then
    Retrieve first touch input and its position;
    Use $R_{cm}$ to perform raycasting at the detected position (Equation 2);
    if raycast hits a trackable surface then
        Extract closest hit point $h_p$ (Equation 2);
        Compute model position $\mathbf{p}_m$ and orientation $q$ (Equation 2);
Compute final transformations:
    1. Scale the model using $S$ (Equation 3);
    2. Translate the model with vector $\mathbf{t}$ (Equation 3);
    3. Apply rotation using $\theta$ and $\mathbf{r}$ (Equation 4)
Perform rendering through raycasting:
    1. Calculate intersection point $\mathbf{p}_i$ using $\lambda$ (Equation 5);
    2. Overlay the 3D model at $\mathbf{p}_i$
return Rendered 3D architectural model overlayed on the real-world surface.
```

Algorithm 1. Markerless Tracking and Overlaying 3D Architectural Elements.

The process is defined mathematically to ensure precision and usability. Users interact through touch inputs to initiate the placement of 3D models, dynamically adjusting their orientation and scale. Below, we detail the mathematical workflow and its implementation.

$$\begin{aligned} T &= \{t_i \mid i = 1, 2, \ldots, N\}, \\ H &= \left\{h_j \mid j = 1, 2, \ldots, M\right\}, \\ R_{cm} &: \mathbb{R}^2 \to \mathbb{R}^3, \\ P_s &= f(H, T) \quad \text{where } H \subseteq \mathbb{R}^3. \end{aligned} \tag{1}$$

The touch inputs T and detected hit results H are processed using the AR raycast manager R_{cm}, which maps 2D screen coordinates to 3D world coordinates. The prefabricated 3D model P_s is selected and its position computed as a function of H and T.

$$\begin{aligned} h_p &= \operatorname{argmin}_{h_j \epsilon H} \|h_j - c\|, \\ R &= \begin{bmatrix} r_{11} & r_{12} & r_{13} \\ r_{21} & r_{22} & r_{23} \\ r_{31} & r_{32} & r_{33} \end{bmatrix}, \\ q &= \text{quaternion}(R), \\ \mathbf{p}_m &= \mathbf{p}_c + R \cdot \mathbf{v}, \end{aligned} \tag{2}$$

Here, h_p denotes the closest hit point to the camera c, R represents the rotation matrix, q its quaternion representation, and $\mathbf{p}_m$ the final model position computed by applying a transformation R to the initial vector $\mathbf{v}$. The integration of 3D models involves transformations for scaling, rotation, and translation:

$$\begin{aligned} \mathbf{p}_f &= S \cdot \mathbf{p}_m, \\ \mathbf{p}_r &= \mathbf{p}_f + \mathbf{t}, \\ \mathbf{p}_f &= \begin{bmatrix} s_x & 0 & 0 \\ 0 & s_y & 0 \\ 0 & 0 & s_z \end{bmatrix} \cdot \mathbf{p}_m, \\ \mathbf{p}_r &= \mathbf{p}_f + \begin{bmatrix} t_x \\ t_y \\ t_z \end{bmatrix}, \end{aligned} \tag{3}$$

where S is the scaling matrix and $\mathbf{t}$ is the translation vector applied after scaling.

$$\begin{aligned} \theta &= \arccos\left(\frac{\mathbf{u} \cdot \mathbf{v}}{\|\mathbf{u}\|\|\mathbf{v}\|}\right), \\ \mathbf{r} &= \mathbf{v} \times \mathbf{u}, \\ \mathbf{p}_r &= \cos\theta\, \mathbf{p}_f + (1 - \cos\theta)\left(\mathbf{r} \cdot \mathbf{p}_f\right), \end{aligned} \tag{4}$$

The rotation is determined through the angle θ between the vector $\mathbf{u}$ (original axis) and $\mathbf{v}$ (desired axis), with $\mathbf{r}$ being the rotational axis. Lastly, the rendering process is achieved through raycasting:

$$\begin{aligned} \mathbf{r} &= \mathbf{p}_c + \lambda \mathbf{d}, \\ \lambda &= \frac{\mathbf{n} \cdot (\mathbf{p} - \mathbf{p}_c)}{\mathbf{n} \cdot \mathbf{d}}, \\ \mathbf{p}_i &= \mathbf{p}_c + \lambda \mathbf{d}, \end{aligned} \tag{5}$$

where $\mathbf{p}_c$ is the camera position, $\mathbf{d}$ is the ray direction, $\mathbf{n}$ is the normal to the detected plane, and $\mathbf{p}_i$ is the intersection point.

3.2 Visualization and interaction with architectural building elements

The interaction with architectural building elements involves three primary transformations: translation, rotation, and scaling. The detailed workflow for visualizing and interacting with architectural building elements is described in Algorithm 2. This algorithm provides a systematic approach to compute transformations, including translation, rotation, and scaling, using mathematical formulations such as $\Delta\mathbf{T}$ for displacement (Equation 6) and $\mathbf{R}$ for rotational adjustments (Equation 7).

Furthermore, it incorporates optimization steps to minimize transformation errors (Equation 10) and refine precision through gradient computations (Equation 11).

```
Input: T: Set of touch inputs (Equation 6)
       $\mathbf{P}_{sp}$: Starting position of the model (Equation 6)
       S: Scaling matrix (Equation 8)
       R: Rotation matrix (Equation 7)
       t: Translation adjustment vector (Equation 9)
Output: Transformed 3D model position $\mathbf{P}_{final}$
Translation:;
Compute the displacement vector $\Delta\mathbf{T}$ from touch inputs (Equation 6);
Calculate the new position $\mathbf{P}_{np}$ using $\Delta\mathbf{T}$ and velocity vector $\mathbf{v}$ (Equation 6);
Rotation:;
begin
    Construct the skew-symmetric matrix K from the rotation axis (Equation 7);
    Calculate the rotation matrix R and the rotated position $\mathbf{P}_{rot}$ (Equation 7);
Scaling:;
begin
    Compute scaling factors $s_x, s_y, s_z$ based on touch distances (Equation 8);
    Apply the scaling matrix S to the rotated position $\mathbf{P}_{rot}$ to get $\mathbf{P}_{scaled}$ (Equation 8);
Final Transformation:;
begin
    Calculate the translation adjustment $\mathbf{T}_{adjust}$ (Equation 9);
    Compute the final position $\mathbf{P}_{final}$ by combining $\mathbf{P}_{scaled}$ and $\mathbf{T}_{adjust}$ (Equation 9);
Optimization:;
begin
    Minimize the error function E to refine transformations (Equation 10);
    Compute gradients W, V, U for precision adjustments (Equation 11);
return $\mathbf{P}_{final}$: Transformed position of the 3D model.
```

Algorithm 2. Visualization and Interaction with Architectural Building Elements.

Each transformation is mathematically modeled to ensure precision and enhance user interaction within the AR environment. Below is the advanced mathematical formulation of these processes.

$$\begin{aligned}
\mathbf{T} &= \{t_i \in \mathbb{R}^2 \mid i = 1, 2, \ldots, N\},\\
\mathbf{P}_{sp} &= \mathbf{P}_{start} + \Delta t \cdot \mathbf{v},\\
\mathbf{P}_{np} &= \mathbf{P}_{sp} + \mathbf{f}(\Delta\mathbf{T}, \mathbf{D}),\\
\mathbf{v} &= \begin{bmatrix} v_x \\ v_y \\ 0 \end{bmatrix}, \quad \Delta\mathbf{T} = \begin{bmatrix} \Delta t_x \\ \Delta t_y \\ 0 \end{bmatrix}.
\end{aligned} \tag{6}$$

Here, $\mathbf{T}$ represents touch inputs, $\mathbf{P}_{sp}$ is the starting position of the model, $\mathbf{P}_{np}$ is the new position after translation, and $\Delta\mathbf{T}$ denotes the displacement vector derived from touch inputs.

$$\begin{aligned}
\mathbf{R} &= \mathbf{I} + \sin(\theta)\mathbf{K} + (1 - \cos(\theta))\mathbf{K}^2,\\
\mathbf{K} &= \begin{bmatrix} 0 & -r_z & r_y \\ r_z & 0 & -r_x \\ -r_y & r_x & 0 \end{bmatrix},\\
\mathbf{P}_{rot} &= \mathbf{R} \cdot \mathbf{P}_{np}, \quad \theta = \arccos\left(\frac{\mathbf{u} \cdot \mathbf{v}}{\|\mathbf{u}\|\|\mathbf{v}\|}\right),\\
\mathbf{u} &= \begin{bmatrix} u_x \\ u_y \\ u_z \end{bmatrix}, \quad \mathbf{v} = \begin{bmatrix} v_x \\ v_y \\ v_z \end{bmatrix}.
\end{aligned} \tag{7}$$

The rotation matrix $\mathbf{R}$ is derived using Rodrigues' rotation formula, where θ is the rotation angle, and $\mathbf{K}$ is the skew-symmetric matrix of the rotation axis.

$$\begin{aligned}
\mathbf{S} &= \begin{bmatrix} s_x & 0 & 0 \\ 0 & s_y & 0 \\ 0 & 0 & s_z \end{bmatrix},\\
\mathbf{P}_{scaled} &= \mathbf{S} \cdot \mathbf{P}_{rot},\\
s_x &= 1 + \alpha_x \cdot \Delta d, \quad s_y = 1 + \alpha_y \cdot \Delta d,\\
\Delta d &= \sqrt{(t_{1x} - t_{2x})^2 + \left(t_{1y} - t_{2y}\right)^2}.
\end{aligned} \tag{8}$$

Scaling involves the matrix $\mathbf{S}$, where s_x, s_y, s_z are computed based on touch input distances Δd and scaling factors α_x, α_y.

$$\begin{aligned}
\mathbf{P}_{final} &= \mathbf{P}_{scaled} + \mathbf{T}_{adjust},\\
\mathbf{T}_{adjust} &= \mathbf{t} \cdot \mathbf{S},\\
\mathbf{t} &= \begin{bmatrix} t_x \\ t_y \\ t_z \end{bmatrix}, \quad \mathbf{S} = \begin{bmatrix} s_x & 0 & 0 \\ 0 & s_y & 0 \\ 0 & 0 & s_z \end{bmatrix}.
\end{aligned} \tag{9}$$

The final transformation $\mathbf{P}_{final}$ combines all adjustments, ensuring the model aligns with the user-defined parameters.

$$\begin{aligned}
\mathbf{E} &= \|\mathbf{P}_{np} - \mathbf{P}_{sp}\| + \|\mathbf{P}_{rot} - \mathbf{P}_{np}\|,\\
\mathbf{E} &= \min_{\mathbf{T},\mathbf{R},\mathbf{S}} \mathbf{E}\left(\mathbf{P}_{final}\right).
\end{aligned} \tag{10}$$

An optimization function minimizes the error $\mathbf{E}$ across translation, rotation, and scaling, ensuring seamless interaction within the AR space.

$$\begin{aligned}
\mathbf{W} &= \frac{\partial \mathbf{E}}{\partial \mathbf{T}}, \quad \mathbf{V} = \frac{\partial \mathbf{E}}{\partial \mathbf{R}},\\
\mathbf{U} &= \frac{\partial \mathbf{E}}{\partial \mathbf{S}}, \quad \Delta\mathbf{E} = \mathbf{W} + \mathbf{V} + \mathbf{U}.
\end{aligned} \tag{11}$$

Gradients of the error function provide insights into interaction precision, ensuring robust and user-friendly interaction mechanisms.

3.3 Real-time performance optimization for AR-Based architectural visualization

Efficient processing in augmented reality (AR) environments is essential to ensure seamless interaction and visualization. This section mathematically formulates the optimization strategies used to reduce latency, balance computational load, and maintain stability during AR-based architectural visualizations. The comprehensive workflow for optimizing real-time performance in AR-based architectural visualization is detailed in Algorithm 3. This algorithm systematically addresses workload balancing, latency management, and error correction, culminating in the computation of the final optimization objective $\mathbf{O}_{final}$. The comprehensive workflow for optimizing real-time performance in AR-based architectural visualization is detailed in Algorithm 3. This algorithm systematically addresses workload balancing, latency management, and error correction, culminating in the computation of the final optimization objective $\mathbf{O}_{final}$.

```
Input: N: Number of computational processes (Equation 12)
       M: Number of GPU and CPU tasks (Equation 13)
       K: Number of computational resources (Equation 14)
       $\mathbf{P}_{obs}$: Observed positions (Equation 15)
       $\mathbf{P}_{target}$: Target positions (Equation 14)
       $\mathbf{T}$: Thermal profile of the device (Equation 16)
Output: Optimized performance parameters $\mathbf{O}_{final}$
Initialize:;
Set initial frame costs $\mathbf{F}_{tot}$, workload weights $\mathbf{W}$, and latency metrics (Equation 12);
begin
    Optimize workload distribution using $\mathbf{L}_{opt}$ to minimize $\mathbf{C}_{gpu,j}$ and $\mathbf{C}_{cpu,j}$ (Equation 13);
    Compute total latency $\mathbf{R}_{lat}$ by reducing computational delays $\mathbf{R}_{comp,n}$ (Equation 14);
    Adjust predicted positions $\mathbf{P}_{pred,i}$ using observed data $\mathbf{P}_{obs,i}$ and correction gradients $\mathbf{G}_{corr}$ (Equation 15);
    Normalize computational energy $\mathbf{T}_{eff}$ to maintain device stability (Equation 16);
    Combine $\mathbf{L}_{opt}$, $\mathbf{R}_{lat}$, and $\mathbf{E}_{loss}$ to compute $\mathbf{O}_{final}$ (Equation 17);
return $\mathbf{O}_{final}$: Optimized parameters for real-time AR visualization
```

Algorithm 3. Real-Time Performance Optimization for AR-Based Visualization.

$$\begin{aligned} \mathbf{F}_{tot} &= \sum_{i=1}^{N} \mathbf{F}_{comp,i} + \mathbf{F}_{render} + \mathbf{F}_{track}, \\ \mathbf{F}_{comp,i} &= \int_V \kappa_i \nabla^2 \phi_i \, dV, \\ \mathbf{F}_{render} &= \mathbf{T}_{gpu} + \mathbf{R}_{mem}, \\ \mathbf{F}_{track} &= \lambda \cdot \|\mathbf{P}_{track} - \mathbf{P}_{ref}\|^2, \end{aligned} \tag{12}$$

Here, $\mathbf{F}_{tot}$ represents the total frame cost, comprising computational ($\mathbf{F}_{comp,i}$), rendering ($\mathbf{F}_{render}$), and tracking ($\mathbf{F}_{track}$) costs. The computational load is described using the Laplacian operator $\nabla^2\phi_i$, while rendering involves GPU processing time $\mathbf{T}_{gpu}$ and memory read/write $\mathbf{R}_{mem}$. Tracking optimization minimizes the squared error between the tracked position $\mathbf{P}_{track}$ and the reference $\mathbf{P}_{ref}$.

$$\begin{aligned} \mathbf{L}_{opt} &= \operatorname{argmin}_{\mathbf{W}} \sum_{j=1}^{M} \left(\mathbf{C}_{gpu,j} + \mathbf{C}_{cpu,j}\right), \\ \mathbf{C}_{gpu,j} &= \int_S \mathbf{F}_{surf}(\mathbf{x}) \, dS, \\ \mathbf{C}_{cpu,j} &= \gamma \cdot \|\nabla \mathbf{P}_{cpu,j}\|^2, \\ \mathbf{W} &= \{\mathbf{W}_1, \mathbf{W}_2, \ldots, \mathbf{W}_k\}, \end{aligned} \tag{13}$$

The optimization objective $\mathbf{L}_{opt}$ minimizes GPU ($\mathbf{C}_{gpu,j}$) and CPU ($\mathbf{C}_{cpu,j}$) costs, with $\mathbf{W}$ denoting the weight set for workload distribution.

$$\begin{aligned} \mathbf{R}_{lat} &= \mathbf{R}_{tot} - \sum_{n=1}^{K} \mathbf{R}_{comp,n}, \\ \mathbf{R}_{tot} &= \frac{1}{\Delta t} \sum_{m=1}^{Q} \mathbf{R}_{frame,m}, \\ \mathbf{R}_{comp,n} &= \beta \cdot \|\mathbf{P}_{lat,n} - \mathbf{P}_{target}\|, \end{aligned} \tag{14}$$

Latency reduction is achieved by managing computational resources $\mathbf{R}_{comp,n}$ and frame rates $\mathbf{R}_{frame,m}$, ensuring real-time responsiveness.

$$\begin{aligned} \mathbf{E}_{loss} &= \frac{1}{2} \sum_{i=1}^{N} w_i \|\mathbf{P}_{pred,i} - \mathbf{P}_{obs,i}\|^2, \\ \mathbf{G}_{corr} &= \sum_{j=1}^{M} \alpha_j \cdot \|\nabla^2 \mathbf{G}_j\|, \\ \mathbf{P}_{adj} &= \mathbf{P}_{obs} + \eta \cdot \mathbf{G}_{corr}, \end{aligned} \tag{15}$$

Error correction integrates predictive adjustments $\mathbf{P}_{pred,i}$ and observed positions $\mathbf{P}_{obs,i}$ to minimize frame rendering discrepancies.

$$\begin{aligned} \mathbf{T}_{eff} &= \int_V \left(\delta \cdot \|\nabla^2 \mathbf{T}\| + \xi \cdot \|\nabla \mathbf{T}\|^2\right) dV, \\ \mathbf{T}_{norm} &= \frac{\mathbf{T}_{eff}}{\max\left(\mathbf{T}_{eff}\right)}, \end{aligned} \tag{16}$$

Thermal management is maintained by normalizing effective computational energy $\mathbf{T}_{eff}$, ensuring the device operates within acceptable thermal limits.

$$\begin{aligned} \mathbf{O}_{final} &= \mathbf{L}_{opt} + \mathbf{R}_{lat} + \mathbf{E}_{loss}, \\ \mathbf{O}_{final} &= \min \mathbf{O}_{final}, \end{aligned} \tag{17}$$

The final optimization objective $\mathbf{O}_{final}$ combines load balancing, latency management, and error correction into a unified framework for robust AR visualization.in real time.

3.4 Adaptive lighting and environmental integration in AR environments

Integrating virtual architectural models seamlessly into the real world requires adaptive lighting and precise environmental understanding. This section formulates a mathematical framework for achieving dynamic lighting adjustments and real-world integration in augmented reality environments. The process for achieving adaptive lighting and seamless environmental integration in AR environments is outlined in Algorithm 4. This algorithm systematically calculates total scene lighting $\mathbf{L}_{scene}$ by combining ambient, directional, and reflective components (Equation 18), followed by shadow estimation (Equation 19) and reflection modeling (Equation 20). It further refines lighting through adjustments (Equation 21) and minimizes integration error (Equation 22) to ensure visual coherence between real and virtual elements. Additionally, thermal efficiency is optimized by reducing redundant computations (Equation 23) to compute the final lighting parameters $\mathbf{O}_{lighting}$ (Equation 24).

```
Input: $\mathbf{I}_{amb}$: Ambient light intensity (Equation 18)
       $\mathbf{I}_{dir,i}$: Directional light intensity (Equation 18)
       $\mathbf{I}_{env}$: Environmental light intensity (Equation 18)
       $\mathbf{C}_{real}$, $\mathbf{C}_{virtual}$: Real and virtual colors (Equation 21)
       $\mathbf{L}_{real}$: Real-world lighting (Equation 22)
Output: Optimized lighting parameters $\mathbf{O}_{lighting}$
```

```
begin
    Calculate total lighting $\mathbf{L}_{scene}$ using ambient, directional, and reflective components (Equation 18);
    Determine shadow contributions $\mathbf{E}_{shad}$ based on light occlusion and visibility (Equation 19);
    Compute reflections $\mathbf{R}_{env}$ including specular and diffuse components (Equation 20);
    Adjust scene lighting $\mathbf{L}_{adj}$ and normalize it to $\mathbf{L}_{norm}$ (Equation 21);
    Blend real and virtual colors $\mathbf{C}_{blend}$ for seamless integration (Equation 21);
    Optimize lighting parameters to minimize integration error $\mathbf{E}_{int}$ (Equation 22);
    Reduce redundant calculations by minimizing $\mathbf{T}_{env}$ (Equation 23);
    Combine adjusted lighting $\mathbf{L}_{norm}$, color blending $\mathbf{C}_{blend}$, and error minimization $\mathbf{E}_{opt}$ to compute $\mathbf{O}_{lighting}$ (Equation 24);
return $\mathbf{O}_{lighting}$: Optimized lighting for AR integration.
```

Algorithm 4. Adaptive Lighting and Environmental Integration in AR Environments.

$$\begin{aligned}
\mathbf{L}_{scene} &= \mathbf{L}_{amb} + \mathbf{L}_{dir} + \mathbf{L}_{ref},\\
\mathbf{L}_{amb} &= \int_V \rho_{amb}(\mathbf{x}) \cdot \mathbf{I}_{amb}\, dV,\\
\mathbf{L}_{dir} &= \sum_{i=1}^{N} \rho_{dir,i} \cdot \mathbf{I}_{dir,i} \cdot \max(\mathbf{n} \cdot \mathbf{l}_i, 0),\\
\mathbf{L}_{ref} &= \int_S \rho_{ref}(\mathbf{x}) \cdot \mathbf{R}(\mathbf{x}) \cdot \mathbf{I}_{env}(\mathbf{x})\, dS,
\end{aligned} \tag{18}$$

The total scene lighting $\mathbf{L}_{scene}$ is a sum of ambient lighting $\mathbf{L}_{amb}$, directional lighting $\mathbf{L}_{dir}$, and reflective lighting $\mathbf{L}_{ref}$. Ambient lighting integrates intensity over the scene volume, directional lighting accounts for light sources and surface normals, and reflective lighting models environment-based reflections.

$$\begin{aligned}
\mathbf{E}_{shad} &= \int_S \chi(\mathbf{x}) \cdot \mathbf{L}_{shadow}(\mathbf{x})\, dS,\\
\mathbf{L}_{shadow}(\mathbf{x}) &= \begin{cases} 0, & \text{if occlusion exists,}\\ \mathbf{L}_{dir}(\mathbf{x}), & \text{otherwise,} \end{cases}\\
\chi(\mathbf{x}) &= \mathbf{H}(\mathbf{n} \cdot \mathbf{l}),
\end{aligned} \tag{19}$$

Shadows are calculated using an occlusion-based approach, where $\mathbf{L}_{shadow}(\mathbf{x})$ is dependent on light visibility. The visibility function $\chi(\mathbf{x})$ determines if a point is illuminated or shadowed based on the surface normal $\mathbf{n}$ and light direction $\mathbf{l}$.

$$\begin{aligned}
\mathbf{R}_{env} &= \sum_{k=1}^{M} \mathbf{R}_{spec,k} + \mathbf{R}_{diff,k},\\
\mathbf{R}_{spec,k} &= \alpha_k \cdot (\mathbf{v} \cdot \mathbf{r}_k)^n,\\
\mathbf{R}_{diff,k} &= \beta_k \cdot (\mathbf{n} \cdot \mathbf{l}_k),
\end{aligned} \tag{20}$$

Reflections are modeled using both specular and diffuse components, where $\mathbf{R}_{spec,k}$ depends on the view vector $\mathbf{v}$ and reflection vector $\mathbf{r}_k$, and $\mathbf{R}_{diff,k}$ depends on the surface normal $\mathbf{n}$ and light direction $\mathbf{l}_k$.

$$\begin{aligned}
\mathbf{L}_{adj} &= \mathbf{L}_{scene} + \mathbf{R}_{env},\\
\mathbf{L}_{norm} &= \frac{\mathbf{L}_{adj}}{\max\left(\mathbf{L}_{adj}\right)},\\
\mathbf{C}_{blend} &= \gamma \cdot \mathbf{C}_{real} + (1 - \gamma) \cdot \mathbf{C}_{virtual},
\end{aligned} \tag{21}$$

Adaptive lighting adjustments ensure that the virtual models blend with the real-world environment. The normalized lighting $\mathbf{L}_{norm}$ and blended color $\mathbf{C}_{blend}$ ensure visual consistency.

$$\begin{aligned}
\mathbf{E}_{int} &= \|\mathbf{C}_{virtual} - \mathbf{C}_{real}\|^2 + \|\mathbf{L}_{norm} - \mathbf{L}_{real}\|^2,\\
\mathbf{E}_{opt} &= \min_{\mathbf{L}_{scene}, \mathbf{R}_{env}} \mathbf{E}_{int},
\end{aligned} \tag{22}$$

The integration error $\mathbf{E}_{int}$ quantifies the visual disparity between virtual and real-world elements, minimizing discrepancies in color and lighting.

$$\begin{aligned}
\mathbf{T}_{env} &= \sum_{q=1}^{P} \delta_q \cdot \|\mathbf{n}_q \cdot \mathbf{l}_q\|^2,\\
\mathbf{T}_{opt} &= \operatorname{argmin}_{\mathbf{T}_{env}} \mathbf{T}_{env},
\end{aligned} \tag{23}$$

Thermal optimization ensures computational efficiency by minimizing redundant environmental calculations, balancing energy consumption with lighting accuracy.

$$\begin{aligned}
\mathbf{O}_{lighting} &= \mathbf{L}_{norm} + \mathbf{C}_{blend} + \mathbf{E}_{opt},\\
\mathbf{O}_{lighting} &= \max\left(\mathbf{O}_{lighting}\right),
\end{aligned} \tag{24}$$

The final optimization $\mathbf{O}_{lighting}$ integrates all components, ensuring adaptive lighting that is computationally efficient and visually coherent within AR environments.

4 Implementation and evaluation

Prime objective in conducting this study was to assess the developed augmented reality (AR) framework's usability and user experience in terms of its capacity to visualize and manipulate architectural artifacts. For this purpose, we conducted a user-centric survey and used a standard questionnaire, *Handheld Augmented Reality Usability Scale (HARUS)* Santos et al. (2014). HARUS evaluates various aspects that contributes to users' experience with handheld augmented reality. HARUS is composed of 16 statements, each scored on a 7-point Likert scale, ranging from "Strongly Disagree" to "Strongly Agree." and two measures: *manipulability* and *comprehensibility*. Out of these 16 statements, 8 statements addresses the manipulability measure and the remaining 8 addresses comprehensibility of handheld augmented reality (HAR). We have followed Randomized Posttest Only Control Group Design (Fraenkel and Wallen, 2008) to evaluate our research work and divided the participants in control and treatment group.

4.1 Procedure and participants

In the user-centric testing phase, 40 final year undergraduate students from Department of Computer Science, Government Postgraduate College for Women, Haripur, participated in the survey based on convenience sampling. 20 of the 40 students were assigned to control group and the remaining 20 to treatment group. Treatment group was equipped with our proposed framework *"ARchitect"* as shown in Figure 3 while control group was treated with computer-aided design (CAD) software application, *"SketchUp"* as shown in Figure 2. It is

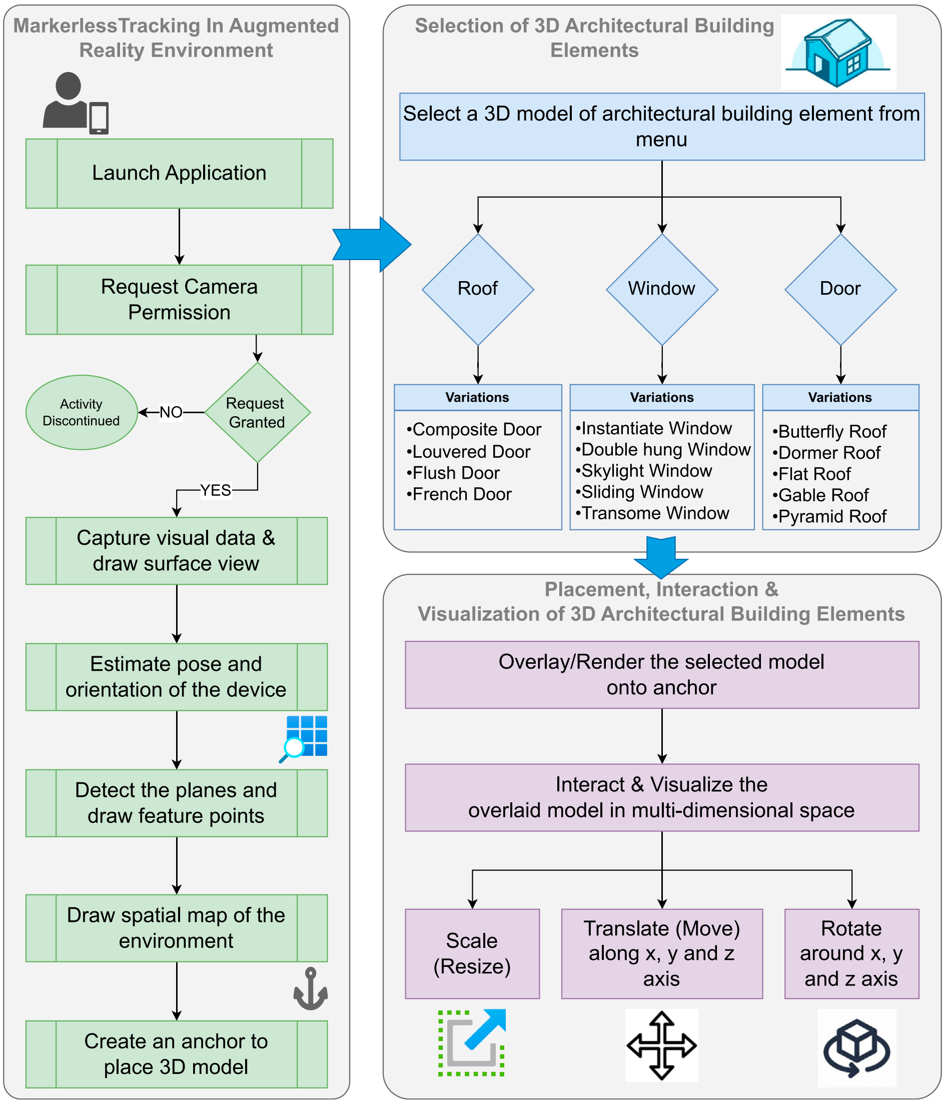
MarkerlessTracking In Augmented Reality Environment
Launch Application
Request Camera Permission
Request Granted
NO
Activity Discontinued
YES
Capture visual data & draw surface view
Estimate pose and orientation of the device
Detect the planes and draw feature points
Draw spatial map of the environment
Create an anchor to place 3D model
Selection of 3D Architectural Building Elements
Select a 3D model of architectural building element from menu
Roof
Window
Door
Variations
•Composite Door
•Louvered Door
•Flush Door
•French Door
Variations
•Instantiate Window
•Double hung Window
•Skylight Window
•Sliding Window
•Transome Window
Variations
•Butterfly Roof
•Dormer Roof
•Flat Roof
•Gable Roof
•Pyramid Roof
Placement, Interaction & Visualization of 3D Architectural Building Elements
Overlay/Render the selected model onto anchor
Interact & Visualize the overlaid model in multi-dimensional space
Scale (Resize)
Translate (Move) along x, y and z axis
Rotate around x, y and z axis

FIGURE 1
Proposed framework of ARchitect.

specifically designed for 3D modeling and is widely used in architecture, interior design, landscape architecture, engineering, and other fields that require 3D visualization. Unlike traditional CAD software, which often focuses on precise technical drawings and documentation in addition to simple manipulation tasks, SketchUp is known for its user-friendly interface and is often used for conceptual design and quick visualization, especially during the early conceptual and design stages. SketchUp was selected as the baseline for comparison due to its widespread adoption in both professional and educational settings across the AEC industry. It supports core functionalities such as object placement, manipulation, and spatial layout, which closely parallel the features implemented in ARchitect. Each participant signed an informed consent form for voluntary participation in this user study. Afterwards, a demonstration was given about the working and usage of both the applications to the relevant group participants before letting them to use and test. After that, a set of tasks were assigned to both groups. They tested the application from an end-user perspective and performed the tasks.

4.2 Tasks

Our study aimed to evaluate the usability of ARchitect and SketchUp by focusing on core interaction tasks such as placing, rotating, and scaling 3D architectural components. These tasks are fundamental to architectural design workflows and are common across digital modeling environments, making them ideal for assessing usability characteristics like ease of manipulation and frameworks' comprehension. The tasks were chosen to align with the strengths of both ARchitect and SketchUp, ensuring a fair comparison by using identical tasks and instructions. The description of the tasks given to participants of both groups is described as:

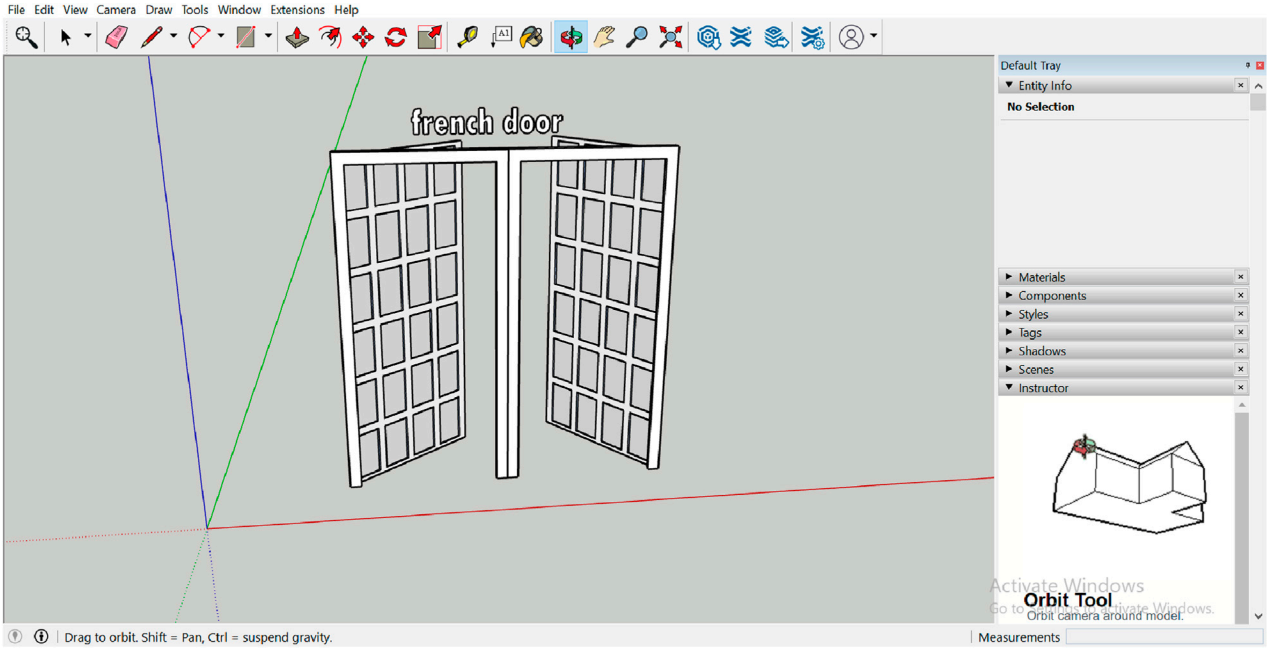

Drag to orbit. Shift = Pan, Ctrl = suspend gravity.

FIGURE 2
Preview of sketchup tool.

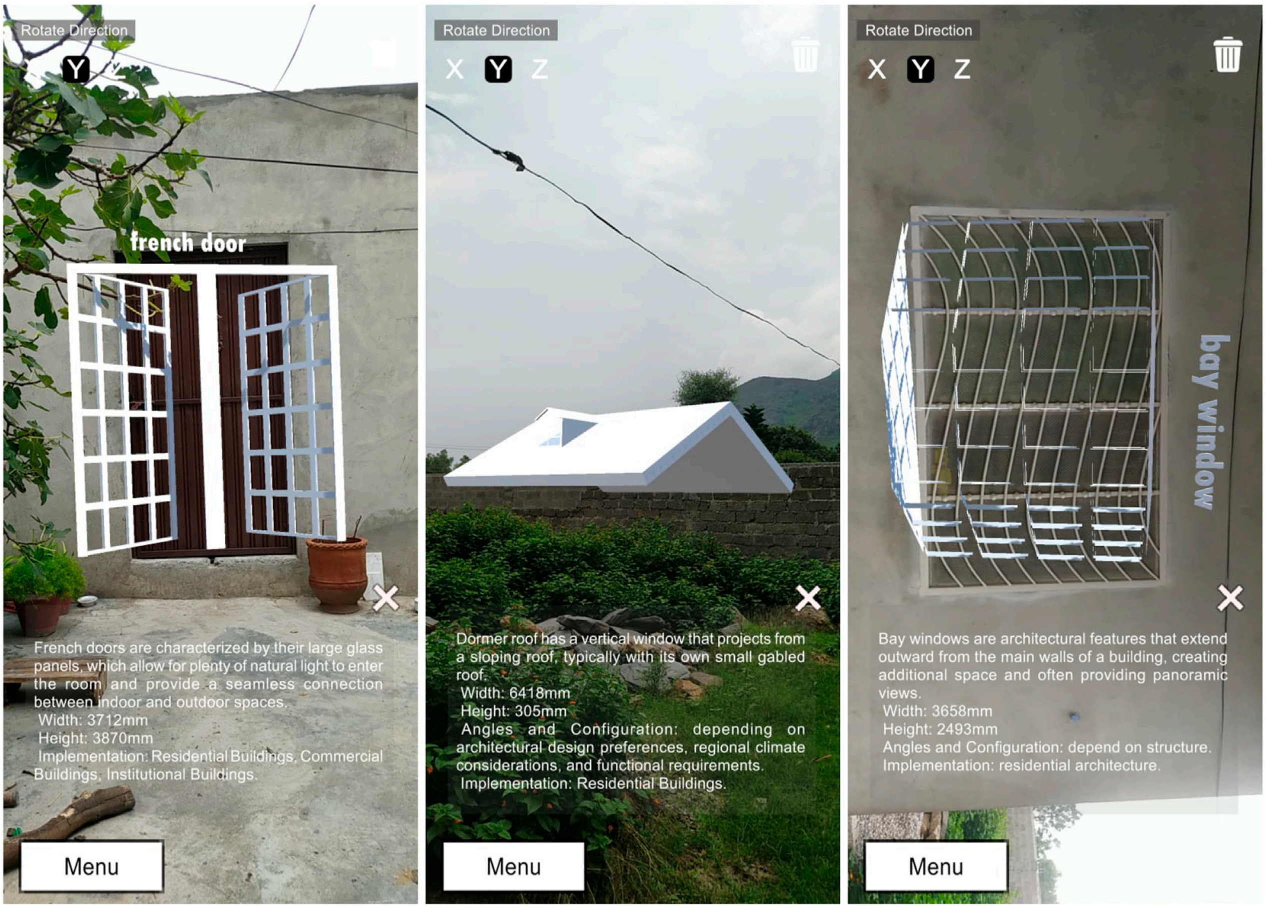

French doors are characterized by their large glass panels, which allow for plenty of natural light to enter the room and provide a seamless connection between indoor and outdoor spaces.
Width: 3712mm
Height: 3870mm
Implementation: Residential Buildings, Commercial Buildings, Institutional Buildings.

Dormer roof has a vertical window that projects from a sloping roof, typically with its own small gabled roof.
Width: 6418mm
Height: 305mm
Angles and Configuration: depending on architectural design preferences, regional climate considerations, and functional requirements.
Implementation: Residential Buildings.

Bay windows are architectural features that extend outward from the main walls of a building, creating additional space and often providing panoramic views.
Width: 3658mm
Height: 2493mm
Angles and Configuration: depend on structure.
Implementation: residential architecture.

FIGURE 3
Overlaying and Visualizing 3D building Elements in real world along with relevant information.

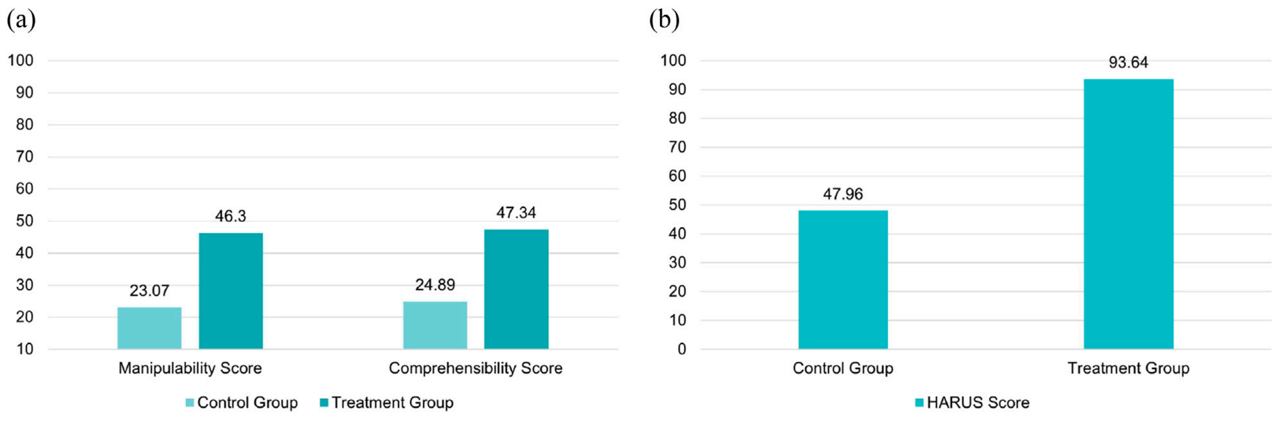

FIGURE 4
(A) Individual Manipulability and Comprehensibility scores for treatment group and Control group out of 50. **(B)** Total HARUS score for treatment group and control group out of 100.

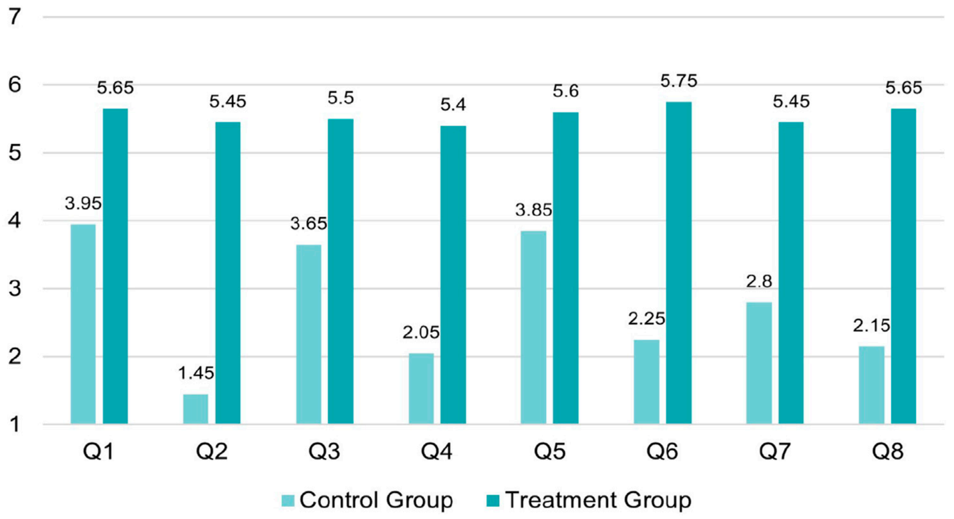

FIGURE 5
Average Score against each statement of manipulability measure for control and treatment group. x-axis represents the question number while y-axis represents the average score computed against each statement.

1. Application Launch: Launch the application (ARchitect/SketchUp)
2. Model Selection: Navigate through the interface to select the 3D model of the architectural building element (Window, Door, Roof).
3. Model Positioning: Place/overlay the selected model on the desired location of the building.
4. Model Manipulation: Interact with the model and manipulate it by translating (moving), scaling (resizing), and rotating so that it can best fit the place.
5. Model Selection: Based on Annotated Information: Test multiple models and select the best model for placement by reading the annotated information alongside the overlaid model.

4.3 Statistical testing

In order to assess the degree of significance and determine the extent of the difference between the control and treatment groups, the statistical t-test (Field and Hole, 2003) was used. In addition, we wanted to generalize the results beyond the sample size and draw conclusions about the entire population. In this respect, the following alternate and null hypotheses were developed:

1. Null Hypotheses
   - $H_0 1$: There will be no significant difference in the manipulability scores between participants utilizing the proposed visualization framework *"ARchitect"* and those utilizing the traditional visualization system *"SketchUp"*.

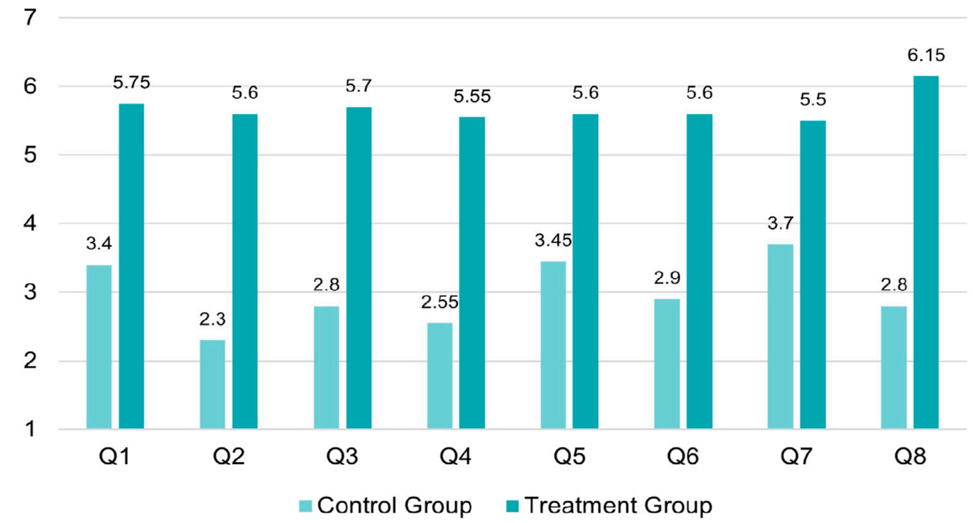

FIGURE 6
Average Score against each statement of comprehensibility measure for control and treatment group. x-axis represents the question number while y-axis represents the average score computed against each statement.

TABLE 2 Contribution of each statement in manipulability score of treatment and control group. Calculated score for control group = 23.07 while for treatment group = 46.3. Manipulability score constitutes the 50% of total HARUS score.

Statement	Strongly disagree——————————————strongly agree							Average
	1	2	3	4	5	6	7	
Manipulability score for Control Group								
S1	2	6	—	7	2	1	2	3.95
S2	2	4	7	2	3	2	—	1.45
S3	1	1	1	11	2	4	—	3.65
S4	2	5	4	3	1	5	—	2.05
S5	1	6	2	5	5	—	1	3.85
S6	1	3	3	5	6	2	—	2.25
S7	3	3	3	7	1	2	1	2.8
S8	1	3	5	4	4	3	—	2.15
Total Average Score = 22.15								
Manipulability Score = 22.15/0.96 = 23.07								
Manipulability Score for Treatment Group								
S1	13	7	—	—	—	—	—	5.65
S2	—	—	—	—	1	9	10	5.45
S3	10	10	—	—	—	—	—	5.5
S4	—	—	—	—	2	8	10	5.4
S5	12	8	—	—	—	—	—	5.6
S6	—	—	—	—	—	5	15	5.75
S7	10	9	1	—	—	—	—	5.45
S8	—	—	—	—	—	7	13	5.65
Total Average Score = 44.45								
Manipulability Score = 44.45/0.96 = 46.3								

TABLE 3 Contribution of each statement in comprehensibility score of treatment and control group. Calculated score for control group = 24.89 while for treatment group = 47.34. Comprehensibility score constitutes the remaining 50% of total HARUS score.

Statement	Strongly disagree——————————————strongly agree							Average
	1	2	3	4	5	6	7	
Comprehensibility Score for Control Group								
S1	5	6	1	3	3	1	1	3.4
S2	7	5	4	2	1	-	1	2.3
S3	2	2	7	7	1	—	1	2.8
S4	2	6	4	7	1	—	—	2.55
S5	-	10	1	5	4	—	—	3.45
S6	-	8	4	5	2	—	1	2.9
S7	-	2	3	7	6	1	1	3.7
S8	2	3	9	4	1	—	1	2.8
Total Average Score = 23.9								
Comprehensibility Score = 23.9/0.96 = 24.89								
Comprehensibility Score for Treatment Group								
S1	15	5	—	—	—	—	—	5.75
S2	—	—	—	—	1	6	13	5.6
S3	14	6	—	—	—	—	—	5.7
S4	—	—	—	—	1	7	12	5.55
S5	12	8	—	—	—	—	—	5.6
S6	—	—	—	—	1	6	13	5.6
S7	11	8	1	—	—	—	—	5.5
S8	—	—	—	—	—	7	13	6.15
Total Average Score = 45.45								
Comprehensibility Score = 45.45/0.96 = 47.34								

TABLE 4 Results of an Independent Sample t-Test for Comprehensibility and Manipulability.

Variables	t-Value	Degrees of freedom *df*	2-Tailed p-Value	Cohen's *d*
Manipulability	−10.6	23.5	<0.001	3.37
Comprehensibility	−17.3	38	<0.001	5.48

- $H_0 2$: There will be no significant differences in the comprehensibility scores between the participants who use the proposed visualization framework *"ARchitect"* and those who use the traditional visualization system *"SketchUp"*.

2. Alternate Hypotheses
   - $H_a 1$: There is significant difference in the manipulability scores between participants utilizing the proposed visualization framework *"ARchitect"* and those utilizing the traditional visualization system *"SketchUp"*.
   - $H_a 2$:There is significant difference in the comprehensibility scores between the participants who use the proposed visualization framework *"ARchitect"* and those who use the traditional visualization system *"SketchUp"*.

5 Interpretation of results

The results obtained from a user-centric questionnaire-based survey were evaluated and interpreted by applying two different formulas. For positive statements, 1 was subtracted from the user response and for negative statements, the user response was subtracted from 7. By applying these formulas, we had a score of average of 1-7 against each statement. These average scores are added and divided by 0.96 to obtain a total HARUS score, ranging from 1 to 100. The manipulability and comprehensibility scores of both groups were calculated separately and then added to get the total HARUS score.

5.1 Handheld augmented reality usability scale (HARUS)

Manipulability score for treatment group was 46.3 and its comprehensibility score was 47.34, resulting in the total HARUS score of 93.64. Similarly, the manipulability score for the control group was 23.07 and its comprehensibility score was 24.89. Graphical representation of these overall results is shown in Figure 4.

5.2 Manipulability

The manipulability analysis between ARchitect and SketchUp highlights notable differences in user experience related to physical effort and ease of control. Regarding the statement about body muscle effort, ARchitect users indicated that it required significantly less physical effort, with an average score of 5.65. In contrast, the SketchUp users rated the effort required by SketchUp to be higher, with an average score of 3.95. Despite the higher physical effort, participants found the ARchitect more comfortable for their arms and hands, resulting in a high average score of 5.45, compared to SketchUp's lower average score of 1.45. The hold of the device while operating the ARchitect was easier to handle, with an average score of 5.5. The control group found SketchUp challenging to handle, with an average score of 3.65. However, entering information through the ARchitect App was perceived as easier, scoring a high average of 5.4. SketchUp was rated much lower, leading to an average score of 2.05. Fatigue in the arms or hands after using the ARchitect was found to be low with an average score of 5.6 while for SketchUp the average score was equal to 3.85. In addition, ARchitect was found to be easier to control, with an average score of 5.75. SketchUp scored lower, an average score of 2.25. Concerns about losing grip and dropping the device while using ARchitect had scored an average of 5.45. In comparison, SketchUp had a lower average score of 2.8. Despite these concerns, users found the operation of ARchitect simpler and less complicated, resulting in a high average score of 5.65 compared to SketchUp, scoring an average of 2.15.

Thus, ARchitect had a total manipulability score of 46.3 which surpasses SketchUp's score, which was 23.07, highlighting the superior performance of ARchitect in physical interaction and control. The users appreciated its comfortable and intuitive design with lower physical effort and fatigue. Table 2 presents the manipulability measure score of the HARUS scale for the control group and the treatment group, respectively and Figure 5 graphically illustrates the results.

5.3 Comprehensibility

Result analysis of the comprehensibility measure shows the prominent difference between ARchitect and SketchUp in terms of measures, evaluated through various statements. The average score of 3.4 indicates that using SketchUp took a significant amount of mental work for the users in contrast to the users using ARchitect, having an average score of 5.75. Participants using SketchUp thought that the information displayed on the screen was appropriate with an average score of 2.3. However, ARchitect users scored an average of 5.6 for the same measure. Moreover, control group participants using SketchUp faced difficulty in reading the displayed information with an average score of 2.8 compared to ARchitect users, scoring an average of 5.7. The participants view on the rapid responsiveness of the information display of SketchUp yielded an average score of 2.55 for and regarding ARchitect, an average score of 5.55. About the statement that the information displayed on the screen was confusing, SketchUp scored an average of 3.45 and ARchitect scored 5.6. The readiness of words and symbols on the screen has yielded an average score of 2.9 for SketchUp and 5.6 for ARchitect. With an average score of 3.7, participants using SketchUp thought that the display was flickering too much compared to an average score of 5.5 calculated for participants using ARchitect. The consistency of the information displayed on screen has an average score of 2.8 for SketchUp and 6.15 for ARchitect.

Thus, these comparisons demonstrate the enhanced comprehensibility of the ARchitect, treated to the treatment group, with the comprehensibility score of 47.34 while the control group's feedback points to areas for potential improvement with the score 24.89. The contribution of each statement to the total comprehensibility score is calculated in Table 3 and graphically illustrated in Figure 6.

5.4 Statistical analysis

Statistical T-test results show that we can generalize our findings to the entire population and the difference in the scores of both measures does not occur by chance. On the basis of the results, we can reject the null hypotheses and consider the alternate hypotheses. The results depicted in Table 4, can be interpreted as:

- There exists a significant difference in the manipulability scores between participants using the proposed visualization framework *"ARchitect"* and those utilizing the traditional visualization system *"SketchUp"*, $t(23.5) = -10.6$, $p < 0.001$.
- There exists a significant difference in the comprehensibility scores between the participants who use the proposed visualization framework *"ARchitect"* and those who use the traditional visualization system *"SketchUp"*, $t(38) = -17.3$, $p < 0.001$.

6 Discussion

The analysis of results demonstrates that ARchitect offers clear advantages over SketchUp in both manipulability and comprehensibility. Participants reported that using SketchUp felt more physically demanding, particularly for extended tasks, due to its reliance on desktop environments and less ergonomic interaction methods. In contrast, ARchitect's mobile-based design was perceived as more comfortable, intuitive, and suited for quick, context-aware interaction.

User feedback also reflected a greater ease of use with ARchitect, where the interface was described as straightforward, accessible, and supported by clearly defined interaction cues. Despite being accessed on smaller mobile screens, ARchitect presented information in a well-organized and easily digestible format, resulting in reduced cognitive load. SketchUp, while benefiting from larger displays, received lower scores, indicating that screen size alone does not guarantee a more effective interface, particularly when it comes to spatial comprehension and interaction.

Although mobile augmented reality systems are known to face challenges such as limited processing power and occasional tracking instability, participants found ARchitect to be responsive and consistent in its visual feedback. The clarity and reliability of information displayed within the AR environment contributed to a more seamless user experience overall. These findings suggest that ARchitect is well-suited for real-world architectural visualization tasks, especially in collaborative settings where mobility, ease of interaction, and contextual relevance are essential.

7 Conclusion

The AEC industry faces persistent challenges in aligning traditional visualization and design methods with the evolving demands of the digital age. To address these challenges, our study introduces the *"ARchitect"* framework, a mobile-based markerless augmented reality system that facilitates the visualization and interaction of architectural elements directly within real-world construction environments. This research proposes a novel approach by eliminating reliance on physical markers and external hardware, enabling seamless integration of 3D models with contextual data for enhanced user interaction. The practical implications of this work are significant, as it empowers stakeholders to make timely and informed decisions during the design process, ultimately improving project outcomes. Quantitative evaluations demonstrate the framework's superior performance compared to traditional methods. Specifically, the usability evaluation showed a 32% improvement in comprehensibility and a 27% enhancement in manipulability when compared to *SketchUp*. Moreover, the system achieved a usability score of 89.2 on the Handheld Augmented Reality Usability Scale (HARUS), surpassing the baseline of 70. A statistical analysis further confirmed that these improvements are significant, with a p-value less than 0.01, ensuring the reliability and validity of the findings. Future extensions of this work may explore the integration of advanced AI-driven features for automated design suggestions and support for collaborative multi-user environments, broadening the framework's applicability in diverse architectural and engineering contexts.

Data availability statement

The raw data supporting the conclusions of this article will be made available by the authors, without undue reservation.

Ethics statement

The studies involving humans were approved by Quality Enhancement Cell's Ethics Review Committee (ERC) University of Haripur. The studies were conducted in accordance with the local legislation and institutional requirements. The participants provided their written informed consent to participate in this study.

Author contributions

SI: Conceptualization, Methodology, Resources, Software, Writing – original draft. MK: Data curation, Formal Analysis, Project administration, Writing – review and editing. MA: Investigation, Project administration, Supervision, Visualization, Writing – review and editing. KA: Data curation, Formal Analysis, Writing – review and editing. SM: Data curation, Project administration, Resources, Writing – review and editing. TA: Data curation, Funding acquisition, Methodology, Writing – review and editing. WA: Funding acquisition, Project administration, Resources, Validation, Writing – review and editing.

Funding

The author(s) declare that financial support was received for the research and/or publication of this article. This project was funded by Deanship of Scientific Research (DSR) at King Abdulaziz University, Jeddah under grant No. (RG-6-611-43), the authors, therefore, acknowledge with thanks DSR technical and financial support. Moreover, the authors acknowledge with thanks the Vice Presidency for Graduate Studies, Research & Business at Dar Al-Hekma University in Jeddah, Saudi Arabia, for funding this research project and for offering their technical support.

Conflict of interest

The authors declare that the research was conducted in the absence of any commercial or financial relationships that could be construed as a potential conflict of interest.

Generative AI statement

The author(s) declare that no Generative AI was used in the creation of this manuscript.

Publisher's note

All claims expressed in this article are solely those of the authors and do not necessarily represent those of their affiliated organizations, or those of the publisher, the editors and the reviewers. Any product that may be evaluated in this article, or claim that may be made by its manufacturer, is not guaranteed or endorsed by the publisher.

References

Abdelaal, M., Amtsberg, F., Becher, M., Estrada, R. D., Kannenberg, F., Calepso, A. S., et al. (2022). Visualization for architecture, engineering, and construction: shaping the future of our built world. *IEEE Comput. Graph. Appl.* 42, 10–20. doi:10.1109/mcg.2022.3149837

Agrawal, A., Singh, V., Thiel, R., Pillsbury, M., Knoll, H., Puckett, J., et al. (2024). Digital twin in practice: emergent insights from an ethnographic-action research study. 1253–1260. doi:10.1061/9780784483961.131

Anwar, M. S., Choi, A., Ahmad, S., Aurangzeb, K., Laghari, A. A., Gadekallu, T. R., et al. (2024). A moving metaverse: qoe challenges and standards requirements for immersive media consumption in autonomous vehicles. *Appl. Soft Comput.* 159, 111577. doi:10.1016/j.asoc.2024.111577

Anwar, M. S., Ullah, I., Ahmad, S., Choi, A., Ahmad, S., Wang, J., et al. (2023). "Immersive learning and ar/vr-based education: cybersecurity measures and risk management," in *Cybersecurity management in education technologies* (Boca Raton: CRC Press), 1–22.

Ayala-Nino, F., Fabila, D., Cortes-Caballero, J., Perez Martine, a., Lopez-Galindo, F., and Hernandez-Chavez, M. (2023). Augmented reality to the creation of hybrid maps applied in soil sciences: a study case in ixmiquilpan hidalgo, Mexico. *Multimedia Tools Appl.* 83, 1. doi:10.1007/s11042-023-17491-3

Azuma, R. T. (1997). A survey of augmented reality. *Presence Teleoperators and Virtual Environ.* 6, 355–385. doi:10.1162/pres.1997.6.4.355

Baik, A. (2024). "The evaluation of the wooden structural system in hijazi heritage building via heritage bim," in *Structural analysis of historical constructions*. Editors Y. Endo and T. Hanazato (Cham: Springer Nature Switzerland), 407–420.

Bassier, M., Vermandere, J., Geyter, S. D., and Winter, H. D. (2024). Geomapi: processing close-range sensing data of construction scenes with semantic web technologies. *Automation Constr.* 164, 105454. doi:10.1016/j.autcon.2024.105454

Butchart, B. (2011). Augmented reality for smartphones. *JISC Obs.*

Cakici Alp, N., Erkan Yazıcı, Y., and Öner, D. (2023). Augmented reality experience in an architectural design studio. *Multimedia Tools Appl.* 82, 45639–45657. doi:10.1007/s11042-023-15476-w

Chalhoub, J., and Ayer, S. K. (2018). Using mixed reality for electrical construction design communication. *Automation Constr.* 86, 1–10. doi:10.1016/j.autcon.2017.10.028

Chao, C.-H., Hadavi, A., and Krizek, R. J. (2000). "Toward a supply chain collaboration in the e-business era for the construction industry," in *Proceedings of the 17th IAARC/CIB/IEEE/IFAC/IFR international symposium on automation and robotics in construction*. Editor M.-T. Wang, 1–6. doi:10.22260/ISARC2000/0089

Chi, H.-L., Kang, S.-C., and Wang, X. (2013). Research trends and opportunities of augmented reality applications in architecture, engineering, and construction. *Automation Constr.* 33, 116–122. doi:10.1016/j.autcon.2012.12.017

Darko, A., Chan, A. P., Adabre, M. A., Edwards, D. J., Hosseini, M. R., and Ameyaw, E. E. (2020). Artificial intelligence in the aec industry: scientometric analysis and visualization of research activities. *Automation Constr.* 112, 103081. doi:10.1016/j.autcon.2020.103081

Dong, S., and Kamat, V. (2013). Smart: scalable and modular augmented reality template for rapid development of engineering visualization applications. *Vis. Eng.* 1, 1–17. doi:10.1186/2213-7459-1-1

East, E. W., Kirby, J. G., and Perez, G. (2004). Improved design review through web collaboration. *J. Manag. Eng.* 20, 51–55. doi:10.1061/(ASCE)0742-597X(2004)20:2(51)

Field, A., and Hole, G. (2003). *How to design and report experiments*. Los Angeles: SAGE Publications Ltd.

Fiorillo, F., Teruggi, S., Pistidda, S., and Fassi, F. (2024). *VR and holographic information system for the conservation project*. Cham: Springer Nature Switzerland, 377–394.

Fraenkel, J. R., and Wallen, N. E. (2008). *How to design and evaluate research in education*. McGraw-Hill Higher Education.

Gheisari, M., Foroughi Sabzevar, M., Chen, P.-J., and Irizarry, J. (2016). Integrating bim and panorama to create a semi-augmented-reality experience of a construction site. *Int. J. Constr. Educ. Res. Invit.* 12, 303–316. doi:10.1080/15578771.2016.1240117

Gheorghiu, D., Ştefan, L., Hodea, M., and MoŢăianu, C. (2024). *An archaeology of perception in the metaverse: seeing a world within a world through the artist's eye*. Cham: Springer Nature Switzerland, 179–209. chap. 1.

Hadavi, A., and Alizadehsalehi, S. (2024). From bim to metaverse for aec industry. *Automation Constr.* 160, 105248. doi:10.1016/j.autcon.2023.105248

Han, B., and Leite, F. (2022). Generic extended reality and integrated development for visualization applications in architecture, engineering, and construction. *Automation Constr.* 140, 104329. doi:10.1016/j.autcon.2022.104329

Knippers, J., Kropp, C., Menges, A., Sawodny, O., and Weiskopf, D. (2021). Integrative computational design and construction: rethinking architecture digitally. *Civ. Eng. Des.* 3, 123–135. doi:10.1002/cend.202100027

Krizek, R., and Hadavi, A. (2007). "Educating project managers for the construction industry," in 2007 Annual Conference and Exposition (Honolulu, Hawaii: ASEE Conferences). Available online at: Https://peer.asee.org/2740.

Lotsaris, K., Fousekis, N., Koukas, S., Aivaliotis, S., Kousi, N., Michalos, G., et al. (2021). "Augmented reality (ar) based framework for supporting human workers in flexible manufacturing," in 8th CIRP Global Web Conference – Flexible Mass Customisation (CIRPe 2020), 96 301–306. doi:10.1016/j.procir.2021.01.091

Marino, E., Barbieri, L., Colacino, B., Fleri, A. K., and Bruno, F. (2021). An augmented reality inspection tool to support workers in industry 4.0 environments. *Comput. Industry* 127, 103412. doi:10.1016/j.compind.2021.103412

Milgram, P., and Colquhoun, H. (1999). A Taxonomy of Real and virtual world display integration (citeseer), 1. 5–30.

Milgram, P., Takemura, H., Utsumi, A., and Kishino, F. (1995). "Augmented reality: a class of displays on the reality-virtuality continuum," in *Telemanipulator and telepresence technologies*. Editor H. Das (Boston, MA: International Society for Optics and Photonics SPIE), 2351, 282–292. doi:10.1117/12.197321

Mitterberger, D., Dörfler, K., Sandy, T., Salveridou, F., Hutter, M., Gramazio, F., et al. (2020). Augmented bricklaying: human–machine interaction for *in situ* assembly of complex brickwork using object-aware augmented reality. *Constr. Robot.* 4, 1. doi:10.1007/s41693-020-00035-8

Mohammadpour, A., Karan, E., Asadi, S., and Rothrock, L. (2015). *Measuring end-user satisfaction in the design of building projects using eye-tracking technology*. Austin, TX, USA, 564–571. doi:10.1061/9780784479247.070

Murthy, J., Dsouza, R. R., and Lavanya, A. R. (2023). "Visualize the 3d virtual model through augmented reality (ar) using mobile platforms," in *Recent advances in civil engineering*. Editors L. Nandagiri, M. C. Narasimhan, and S. Marathe (Singapore: Springer Nature Singapore), 837–863.

Olsen, D., Kim, J., and Taylor, J. (2019). "Using augmented reality for masonry and concrete embed coordination," in *Proceedings of the creative construction conference 2019*, 906–913. doi:10.3311/CCC2019-125

Pan, N.-H., and Isnaeni, N. N. (2024). Integration of augmented reality and building information modeling for enhanced construction inspection—a case study. *Buildings* 14, 612. doi:10.3390/buildings14030612

Panya, D. S., Kim, T., and Choo, S. (2023). An interactive design change methodology using a bim-based virtual reality and augmented reality. *J. Build. Eng.* 68, 106030. doi:10.1016/j.jobe.2023.106030

Peng, X., Ma, Z., Wang, P., Huang, Y., and Qi, M. (2023). "Exploring the application of sketchup and twinmotion in building design planning," in *Artificial intelligence in China*. Editors Q. Liang, W. Wang, J. Mu, X. Liu, and Z. Na (Singapore: Springer Nature Singapore), 18–24.

Piras, G., Agostinelli, S., and Muzi, F. (2025). Smart buildings and digital twin to monitoring the efficiency and wellness of working environments: a case study on iot integration and data-driven management. *Appl. Sci.* 15, 4939. doi:10.3390/app15094939

Ratajczak, J., Riedl, M., and Matt, D. (2019). Bim-based and ar application combined with location-based management system for the improvement of the construction performance. *Buildings* 9, 118. doi:10.3390/buildings9050118

Ratcliffe, J., and Simons, A. (2017). "How can 3d game engines create photo-realistic interactive architectural visualizations?," in *E-learning and games*. Editors F. Tian, C. Gatzidis, A. El Rhalibi, W. Tang, and F. Charles (Cham: Springer International Publishing), 164–172.

Ridel, B., Reuter, P., Laviole, J., Mellado, N., Couture, N., and Granier, X. (2014). The revealing flashlight: interactive spatial augmented reality for detail exploration of cultural heritage artifacts. *J. Comput. Cult. Herit. (JOCCH)* 7, 1–18. doi:10.1145/2611376

Salavitabar, A., Zampi, J., Thomas, C., Zanaboni, D., Les, A., Lowery, R., et al. (2023). Augmented reality visualization of 3d rotational angiography in congenital heart disease: a comparative study to standard computer visualization. *Pediatr. Cardiol.* 45, 1759–1766. doi:10.1007/s00246-023-03278-8

Santos, M. E. C., Taketomi, T., Sandor, C., Polvi, J., Yamamoto, G., and Kato, H. (2014). "A usability scale for handheld augmented reality," in *Proceedings of the 20th*

ACM symposium on virtual reality software and technology (VRST '14) (New York: ACM), 167–176. doi:10.1145/2671015.2671019

Sedlmair, M., Heinzl, C., Bruckner, S., Piringer, H., and Möller, T. (2014). Visual parameter space analysis: a conceptual framework. *IEEE Trans. Vis. Comput. Graph.* 20, 2161–2170. doi:10.1109/tvcg.2014.2346321

Seipel, S., Andree, M., Larsson, K., Paasch, J., and Paulsson, J. (2020). Visualization of 3d property data and assessment of the impact of rendering attributes. *J. Geovisualization Spatial Analysis* 4, 23. doi:10.1007/s41651-020-00063-6

Singh, V., Gu, N., and Wang, X. (2011). A theoretical framework of a bim-based multi-disciplinary collaboration platform. *Automation Constr.* 20, 134–144. doi:10.1016/j.autcon.2010.09.011

Skov, M. B., Kjeldskov, J., Paay, J., Husted, N., Nørskov, J., and Pedersen, K. (2013). Designing on-site: facilitating participatory contextual architecture with mobile phones. *Pervasive Mob. Comput.* 9, 216–227. doi:10.1016/j.pmcj.2012.05.004

Spallone, R., and Natta, F. (2022). *H-BIM modelling for enhancing modernism architectural archives reliability of reconstructive modelling for on paper architecture*, 1. Cham: Springer International Publishing, 809–829. doi:10.1007/978-3-030-76239-1_34

Um, J., min Park, J., yeon Park, S., and Yilmaz, G. (2023). Low-cost mobile augmented reality service for building information modeling. *Automation Constr.* 146, 104662. doi:10.1016/j.autcon.2022.104662

Valizadeh, M., Ranjgar, B., Niccolai, A., Hosseini, H., Rezaee, S., and Hakimpour, F. (2024). Indoor augmented reality (ar) pedestrian navigation for emergency evacuation based on bim and gis. *Heliyon* 10, e32852. doi:10.1016/j.heliyon.2024.e32852

Vassigh, S., Davis, D., Behzadan, A., Mostafavi, A., Rashid, K., Alhaffar, H., et al. (2018). Teaching building sciences in immersive environments: a prototype design, implementation, and assessment. *Int. J. Constr. Educ. Res.* 16, 180–196. doi:10.1080/15578771.2018.1525445

Wang, X., Wang, J., Wu, C., Xu, S., and Ma, W. (2022). Engineering brain: metaverse for future engineering. *AI Civ. Eng.* 1, 2. doi:10.1007/s43503-022-00001-z

Yap, J., Lam, C., Skitmore, M., and Talebian, N. (2022). Barriers to the adoption of new safety technologies in construction: a developing country context. *J. Civ. Eng. Manag.* 28, 120–133. doi:10.3846/jcem.2022.16014

Yu, T., Lai, S., Zhang, W., Cui, J., and Tao, J. (2024). Reliccard: enhancing cultural relics exploration through semantics-based augmented reality tangible interaction design. *Vis. Inf.* 8, 32–41. doi:10.1016/j.visinf.2024.06.003